

Report 3

Object: Targeting, exploration, interpretation and understanding of geothermal sites in Tasmania, Australia, including the area known as the Tamar Conductivity Zone (TCZ).
by Adele Manzella

Pisa, 23rd February 2010

Introduction

On October 2009 I started to work on the data sent in September, asking for the integration of TEM data. The MT data I received referred to 158 sites and were in the form of edi files, containing the spectra resulting from the already performed data analysis. I also received the processed and modeled TEM data acquired over most of this MT sites and on the MT sites previously recorded on Southern profile (191 site data). MT data proved to be very good on most sites; TEM data allowed to correct the static shift of apparent resistivity data.

Decomposition and editing of TCZ MT data

The first step of my analysis has been data rotation and decomposition, as done also in my previous analysis.

Decomposition performed with different algorithms provided very similar results, and error bars were very small in most cases. Decomposed data showed a difference between the two polarization modes on most sites for frequencies lower than 1Hz, proving that there is clear sign of lateral discontinuities. It was therefore very important to define a strike direction and to distinguish between TE and TM mode in order to proceed to 2D modeling phase.

In most sites the vertical magnetic data were good, and the tipper strike was clear. In order to distinguish the two modes I have used mostly the information provided by the tipper strike; therefore I defined as TE the mode having the electric field parallel to the tipper strike direction, and consequently the TM as the other mode. The strike was mainly in the NW-SE direction, as shown in Figs 1-4. The data show a 1D behavior at shallow depth, and a higher dimensionality at frequencies lower than 1 Hz on most cases.

In order to retrieve the maximum number of information from the 2D modeling, I preferred to decompose data instead of rotating them to a fixed direction. I used La Torraca decomposition, but checking also the results of the other decompositions, as already done in the previous report.

After decomposition, data at each site were edited by removing biased data (point located more than 2 standard deviation off the median) and smoothing the curves using D+ algorithm. On the base of tipper strike direction, the TE and TM modes were defined for each site, and data were corrected for static shift by comparison to TEM data modeling results. The resulting curves are presented in Appendix 1.

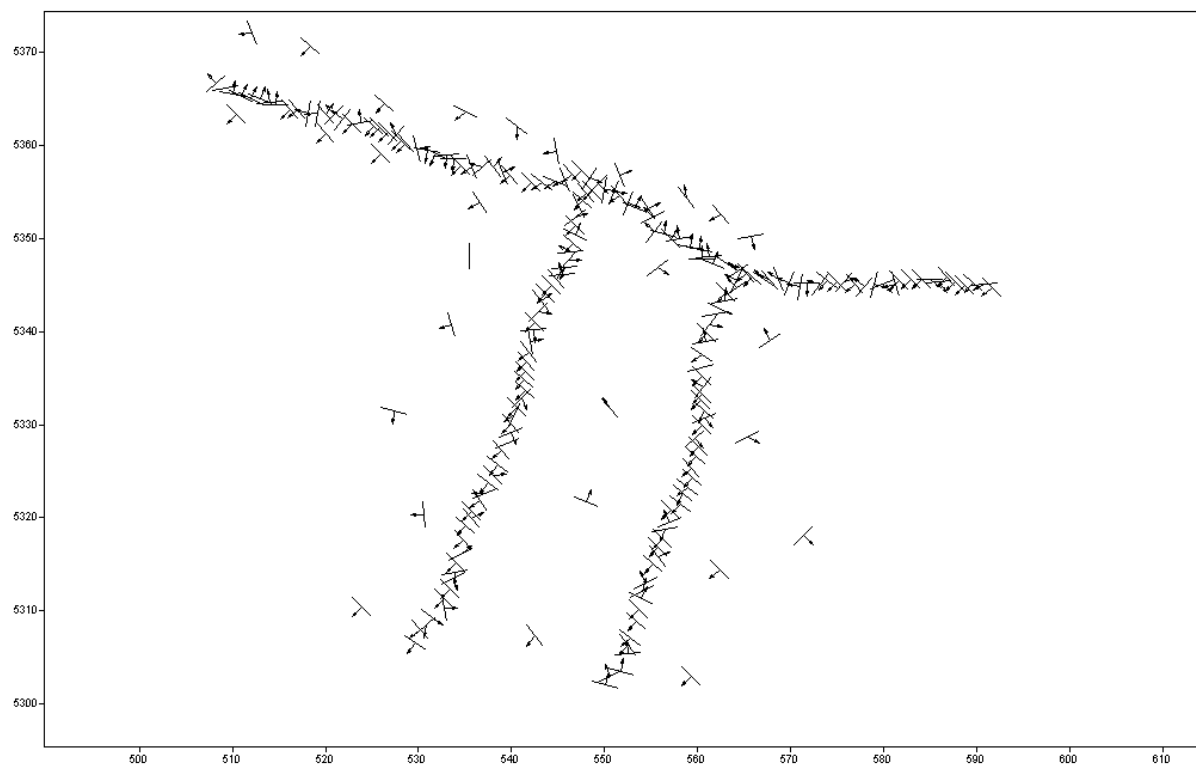


Figure 1. Tipper strike and induction arrow (pointing toward the conductor) at 10 Hz.

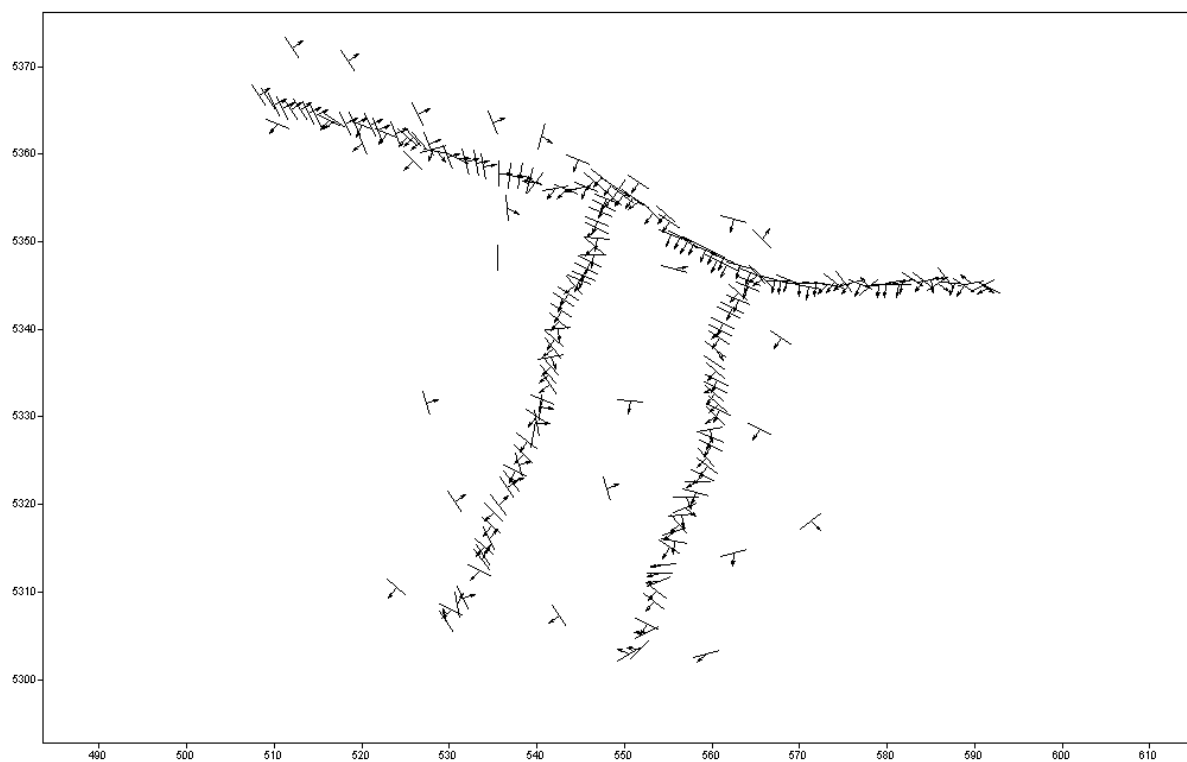


Figure 2. Tipper strike and induction arrow (pointing toward the conductor) at 0.01 Hz.

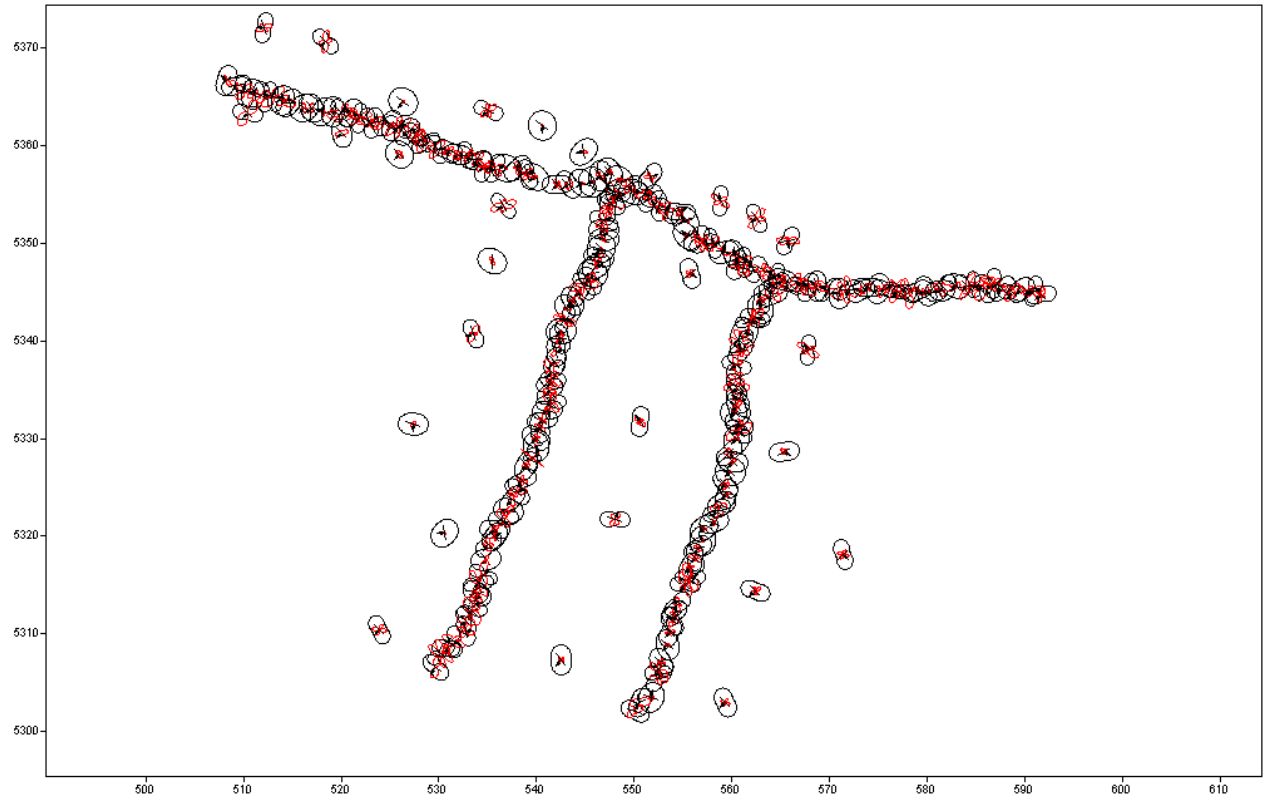


Figure 3. Magnitude polar diagrams of impedance tensor (Z_{xx} in red, Z_{xy} in black) at 10 Hz. The round shape at high frequency implies an almost-1D structure at shallow depth.

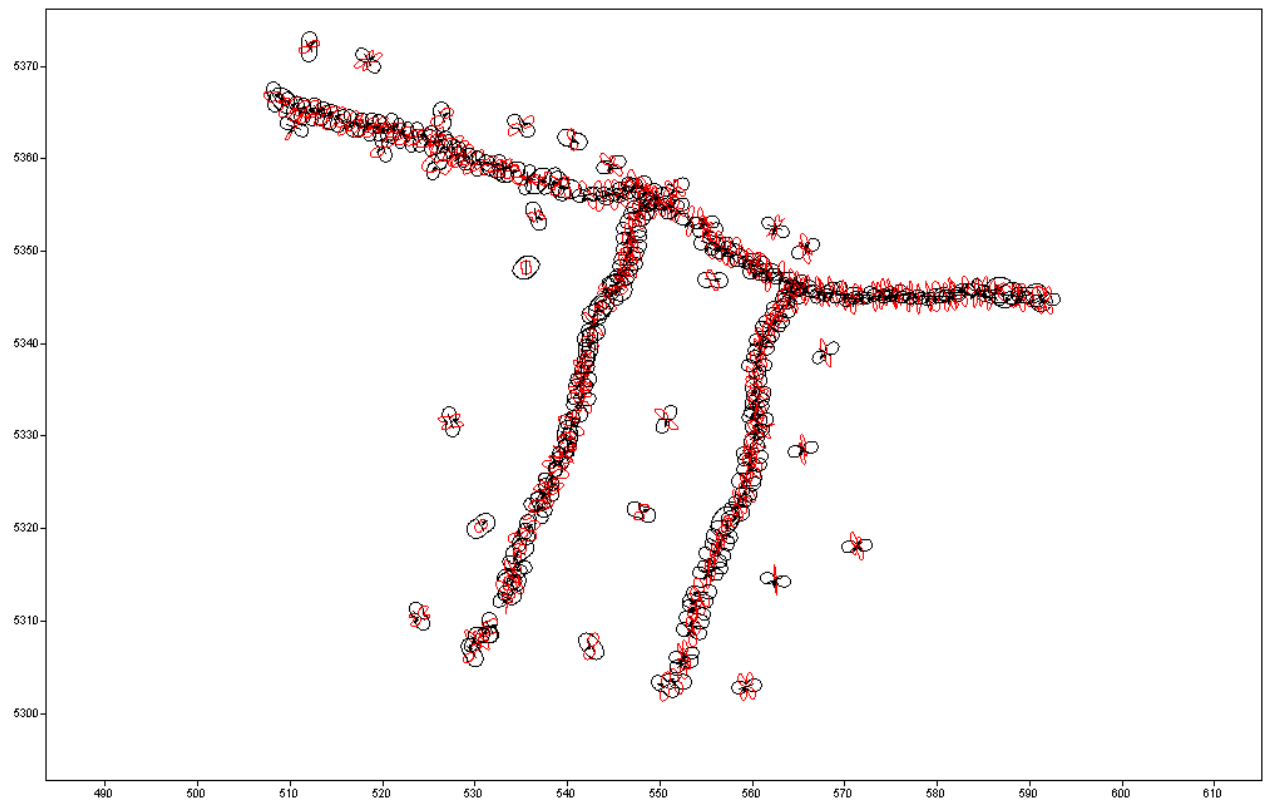


Figure 4. Magnitude polar diagrams of impedance tensor (Z_{xx} in red, Z_{xy} in black) at 0.01 Hz. At the large depth defined by this low frequency a definite strike direction is testified by the direction of elongated magnitude polar diagrams on most sites.

Inversion

All data were 2D inverted using the algorithm of Rodi and Macie (2001) along the profiles shown in Figure 5.

Many models have been computed using various homogeneous starting models (only the sea water was modeled at a certain distance from the area, to simulate the effect of the ocean) and using different parameters for inversion, in order to check and retrieve the most robust features.

I show here the models I obtained for all the profiles, distributed along parallel profiles.

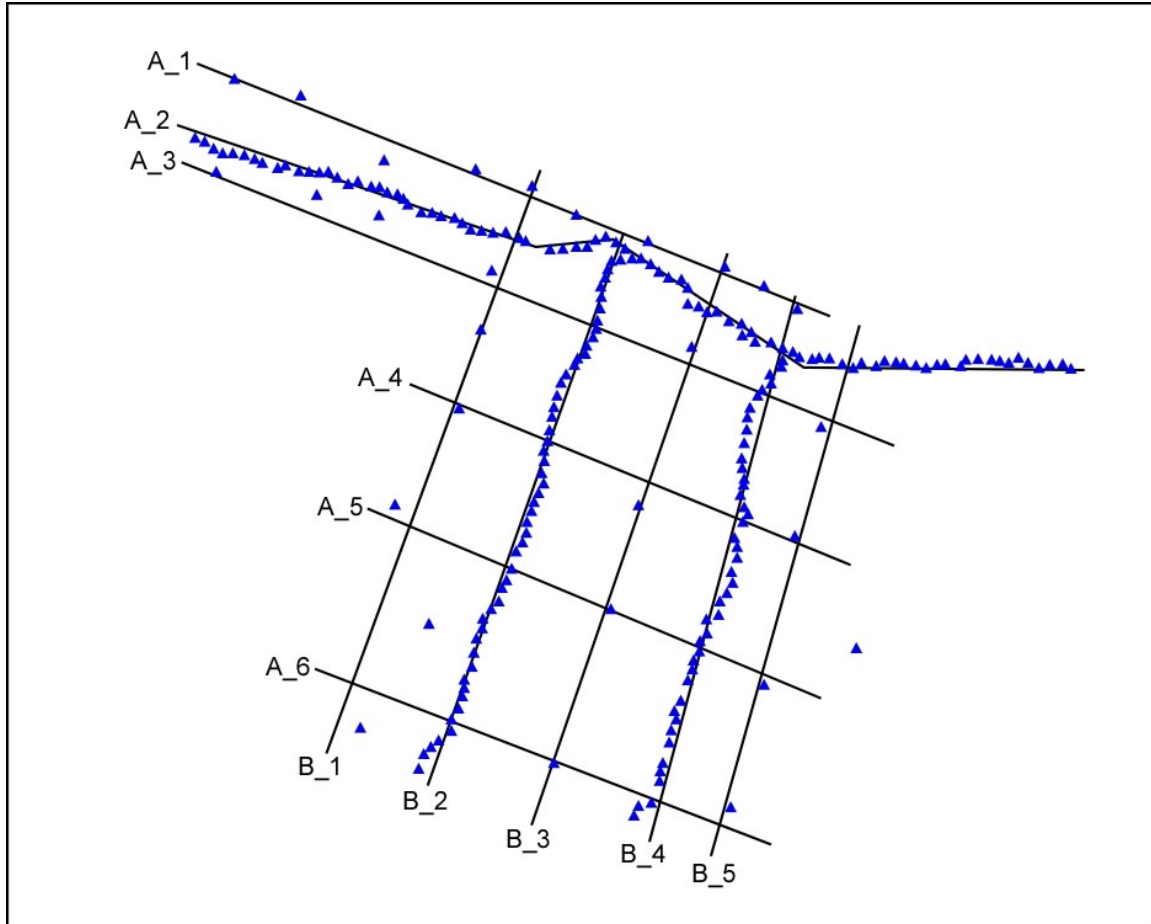


Figure 5. Map showing site location (blue triangles) and the profiles used for this report.

In the NW-SE profile (defined by the letter A), since strike direction is parallel or very close to the direction of the profiles (see Fig. 2), I show only the 2D inversion results of joint TE and TM data, which is the most suited (Fig. 6). On the NNE-SSW profiles (defined by the letter B) I show the 2D inversion results of both the joint TE-TM and the TM data (Figs. 7-8).

In order to perceive the 3D distribution of subsurface resistivity from 2D profiles, I plotted the inversion models along parallel profiles in the same figure, using the same scale and trying to maintain the relative position. The distribution of profiles is shown in a small map in the figure, which is the same map of Fig. 5 but rotated in the direction orthogonal to the profiles. I also plotted the position of the profiles orthogonal to the presented models as dashed lines, to better perceive the relative position.

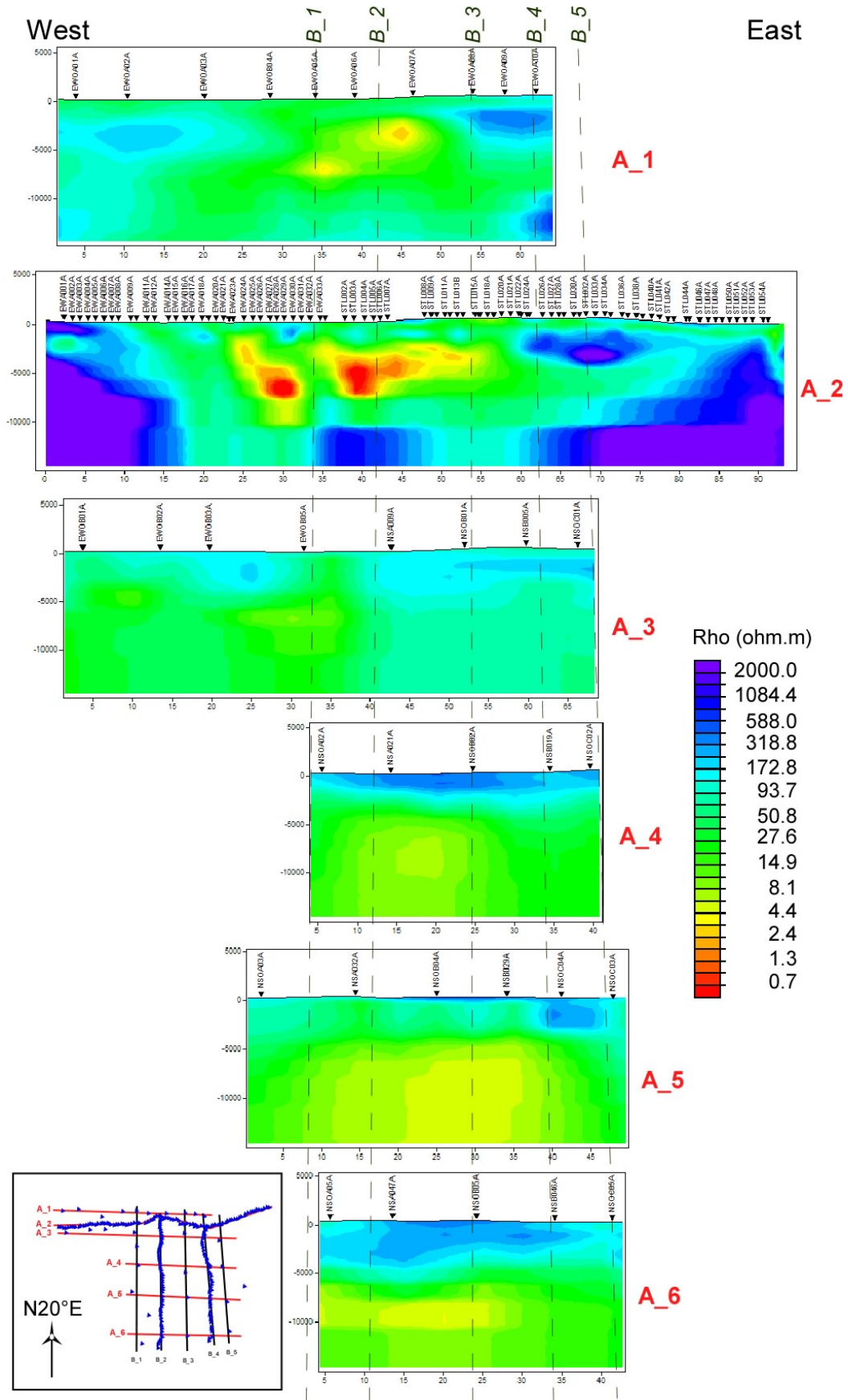


Figure 6. Models obtained by TE-TM data inversion along the NW-SE profiles. Models are distributed in the page as if seen by an observer located on the south-west of the area. The horizontal and vertical scale of the models is the same, to avoid distortion.

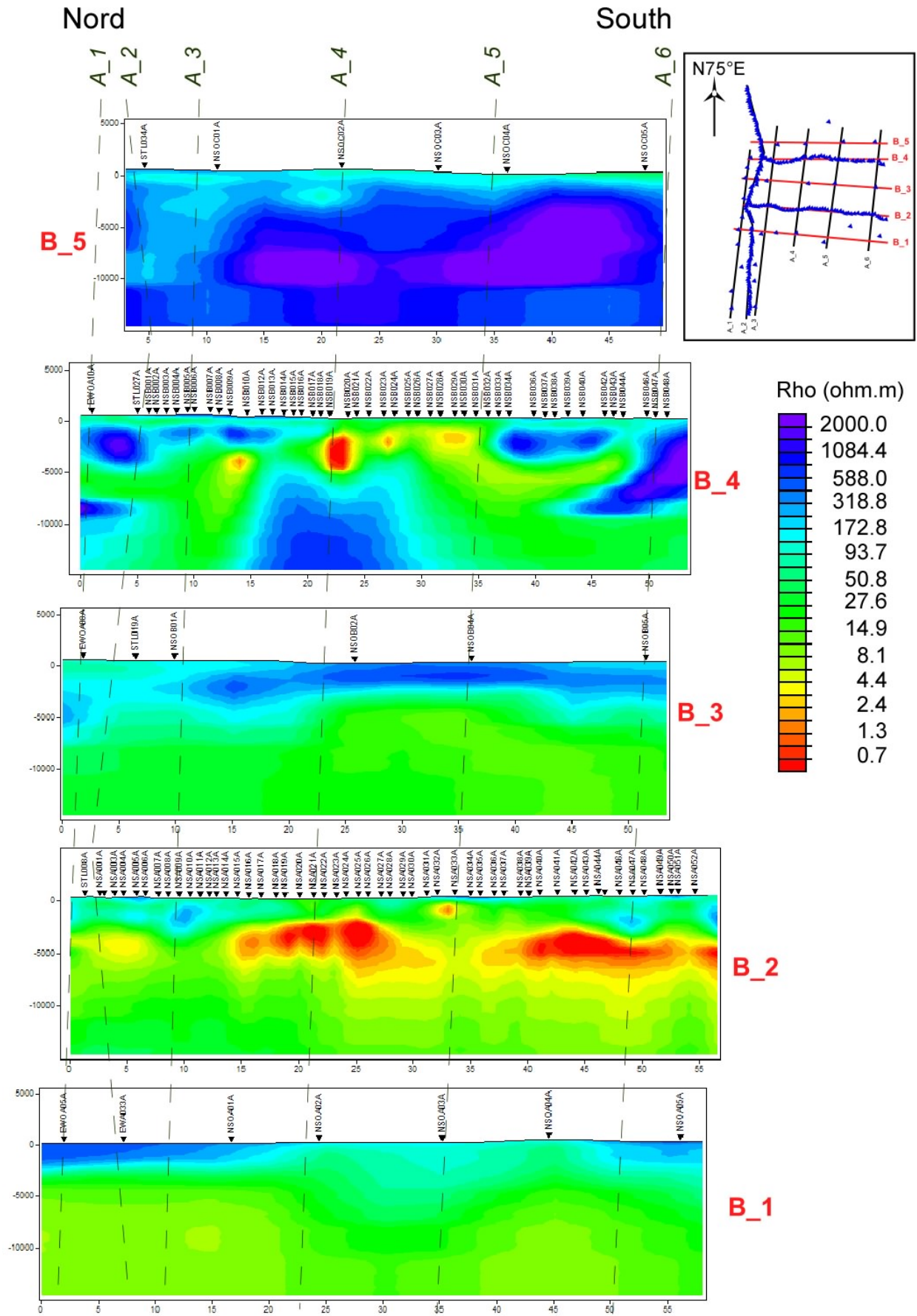


Figure 7. Models obtained by TE-TM data inversion along the NE-SW profiles. Models are distributed in the page as if seen by an observer located on the west of the area. The horizontal and vertical scale of the models is the same, to avoid distortion.

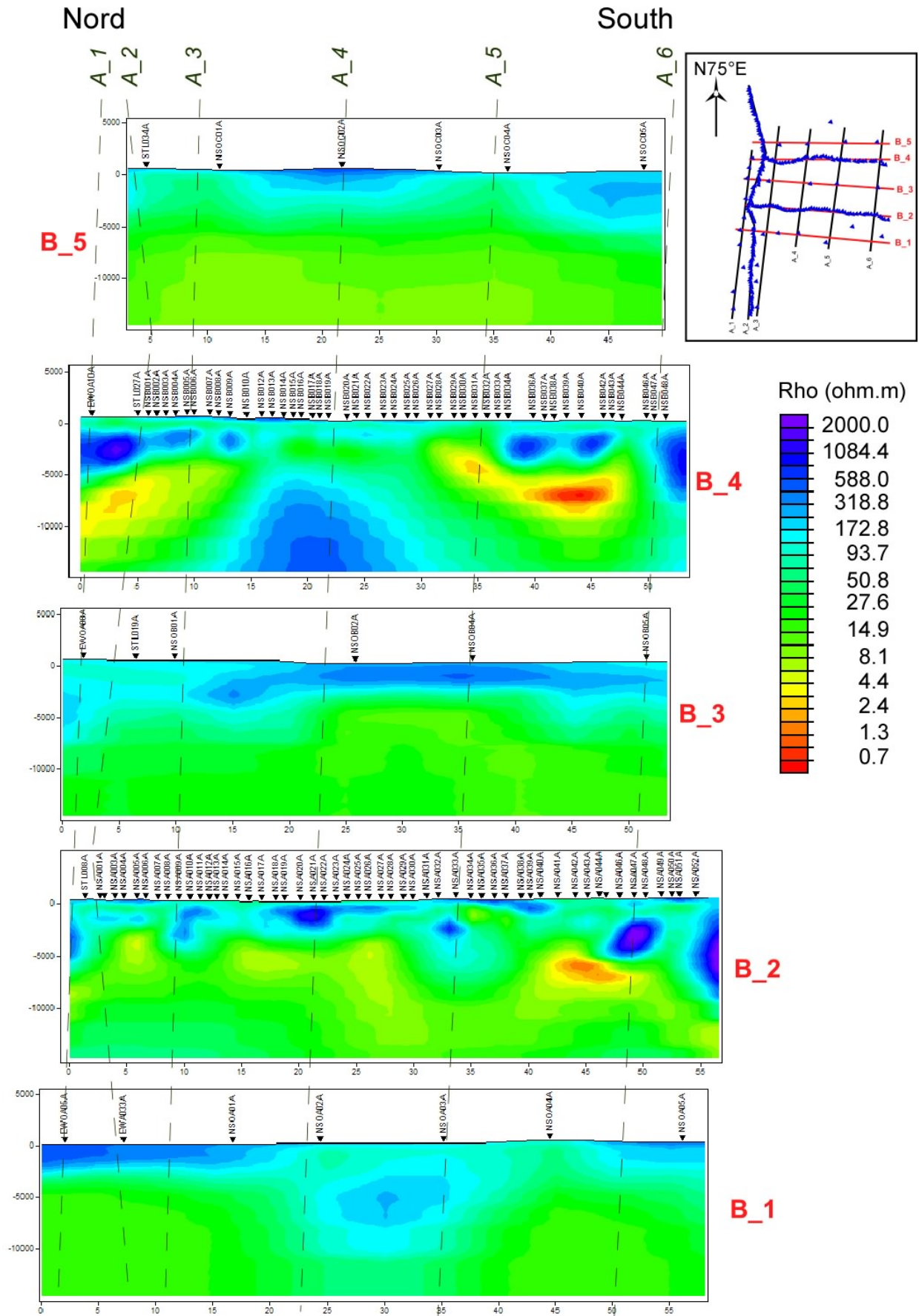


Figure 8. Models obtained by TM data inversion along the NE-SW profiles. Models are distributed in the page as if seen by an observer located on the west of the area. The horizontal and vertical scale of the models is the same, to avoid distortion.

The shown models have been obtained using a priori model of 100 ohm.m (beside the sea, set at 0.3 ohm.m) and a tau parameter equal to 1. The error floor of impedance amplitude and phase has been set to 2% and 1% , respectively, for profiles A_2, B_2 and B_4. The other profiles have error floor values of 5% and 2% for amplitude and phase. Resulting RMS values are listed in Table 1.

<i>Profile name</i>	<i>RMS TE-TM inversion</i>	<i>RMS TM inversion</i>
A_1	4.1	
A_2	18.5	
A_3	11.9	
A_4	17.5	
A_5	19.7	
A_6	10.2	
B_1	13.8	10.5
B_2	7.0	7.0
B_3	9.8	8.5
B_4	6.0	3.2
B_5	5.9	15.7

Table 1. RMS values of the presented models

The horizontal slices of resistivity distribution at different elevation have been obtained by interpolation of modeling results, and are plotted in Figs. 9-15.

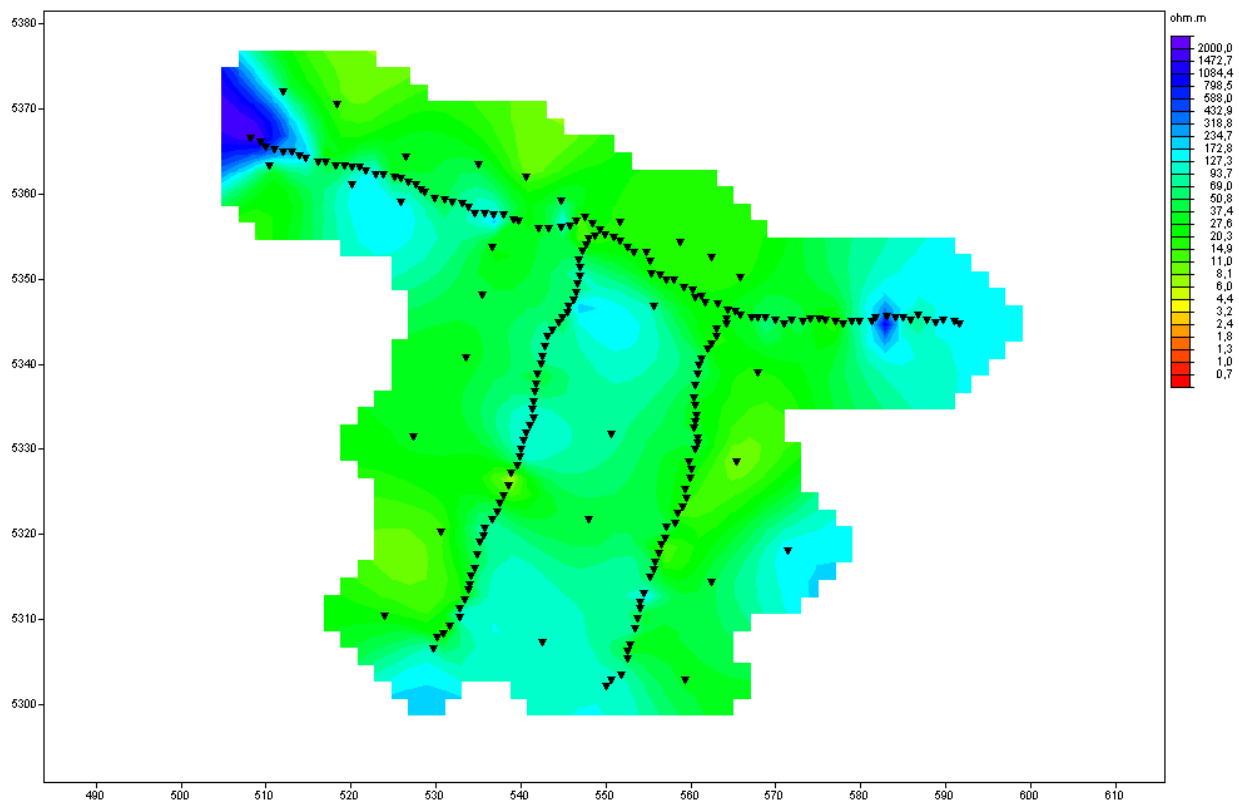


Figure 9. Plan slice of interpolated resistivity values from 2D models obtained by joint inversion of TE and TM data (0 km a.s.l.).

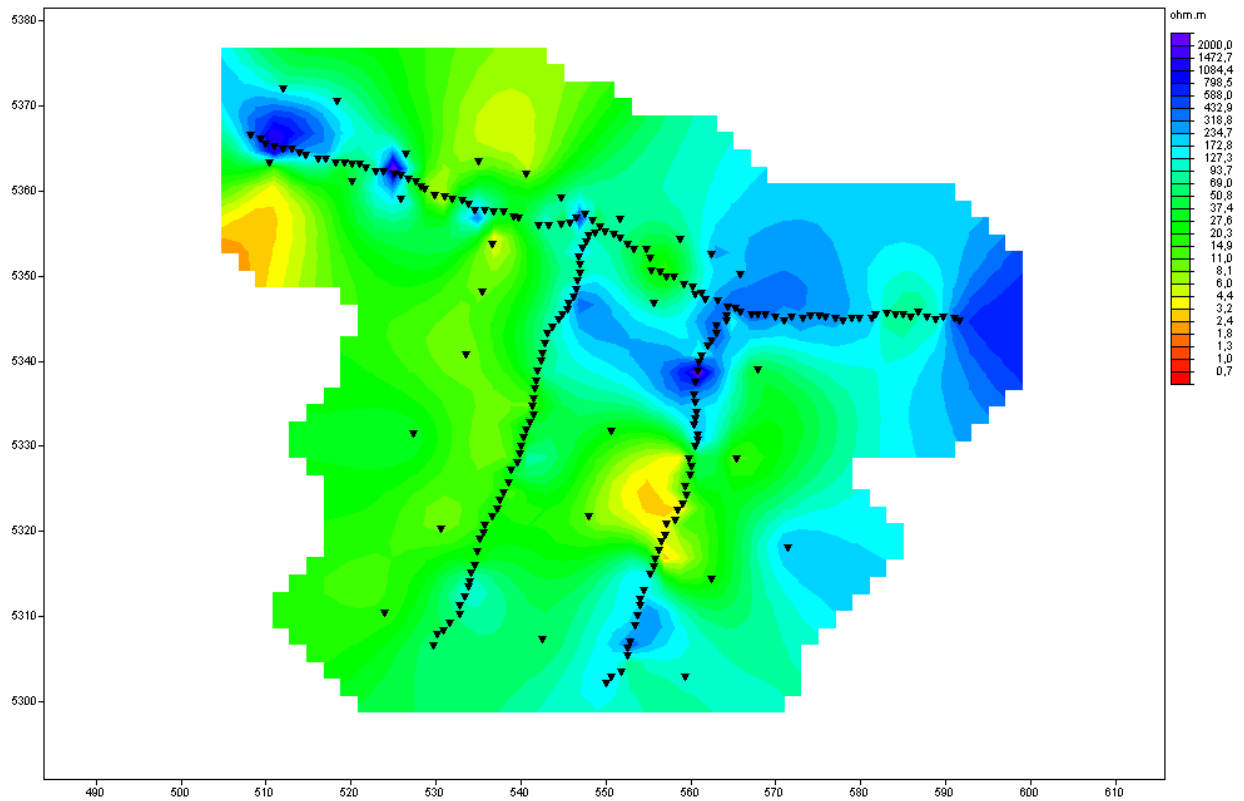


Figure 10. Plan slice of interpolated resistivity values from 2D models obtained by joint inversion of TE and TM data (-1 km a.s.l.).

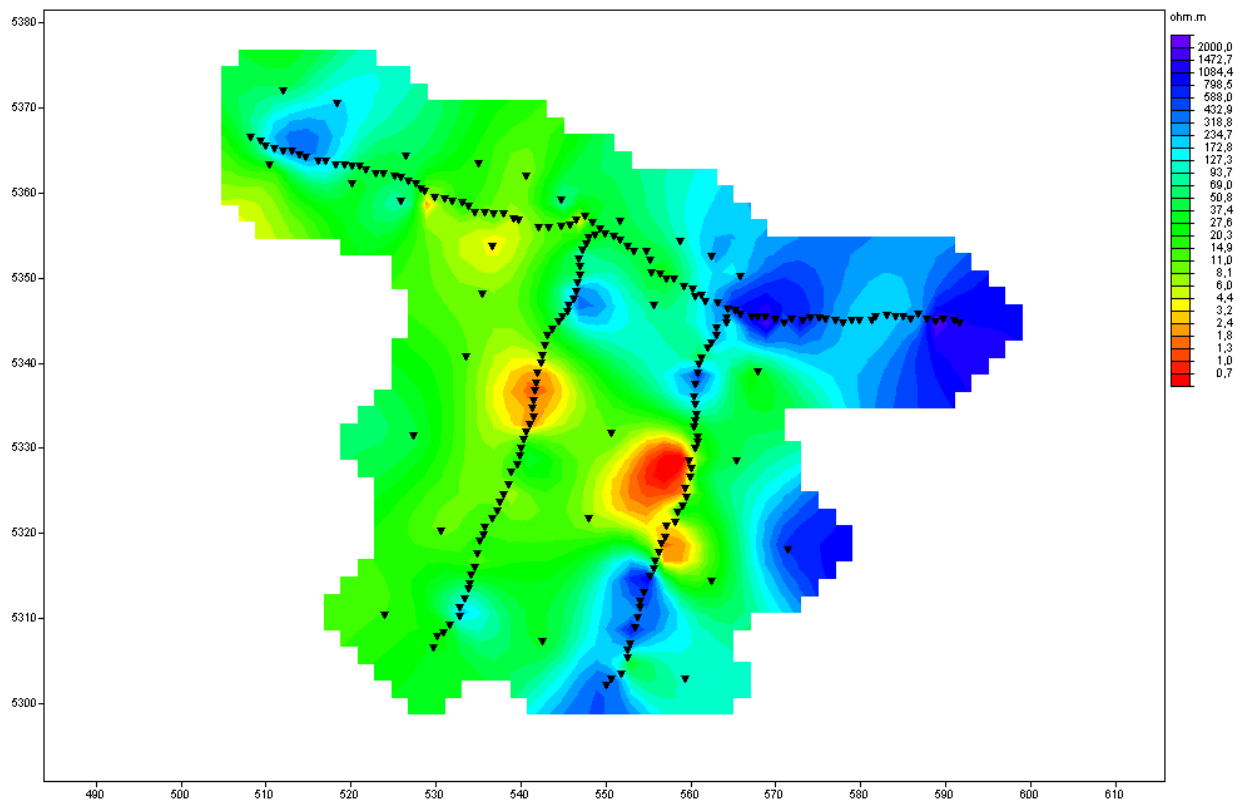


Figure 11. Plan slice of interpolated resistivity values from 2D models obtained by joint inversion of TE and TM data (-2 km a.s.l.).

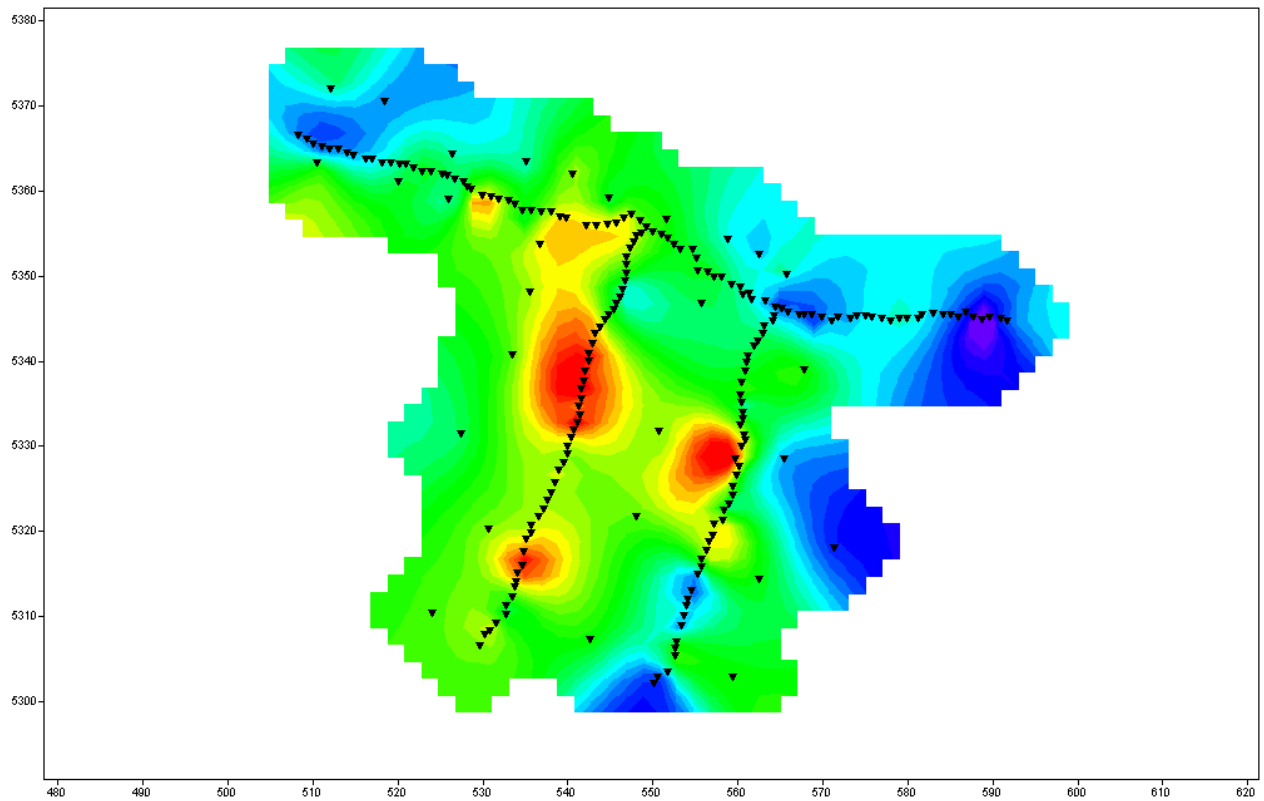


Figure 12. Plan slice of interpolated resistivity values from 2D models obtained by joint inversion of TE and TM data (-3 km a.s.l.).

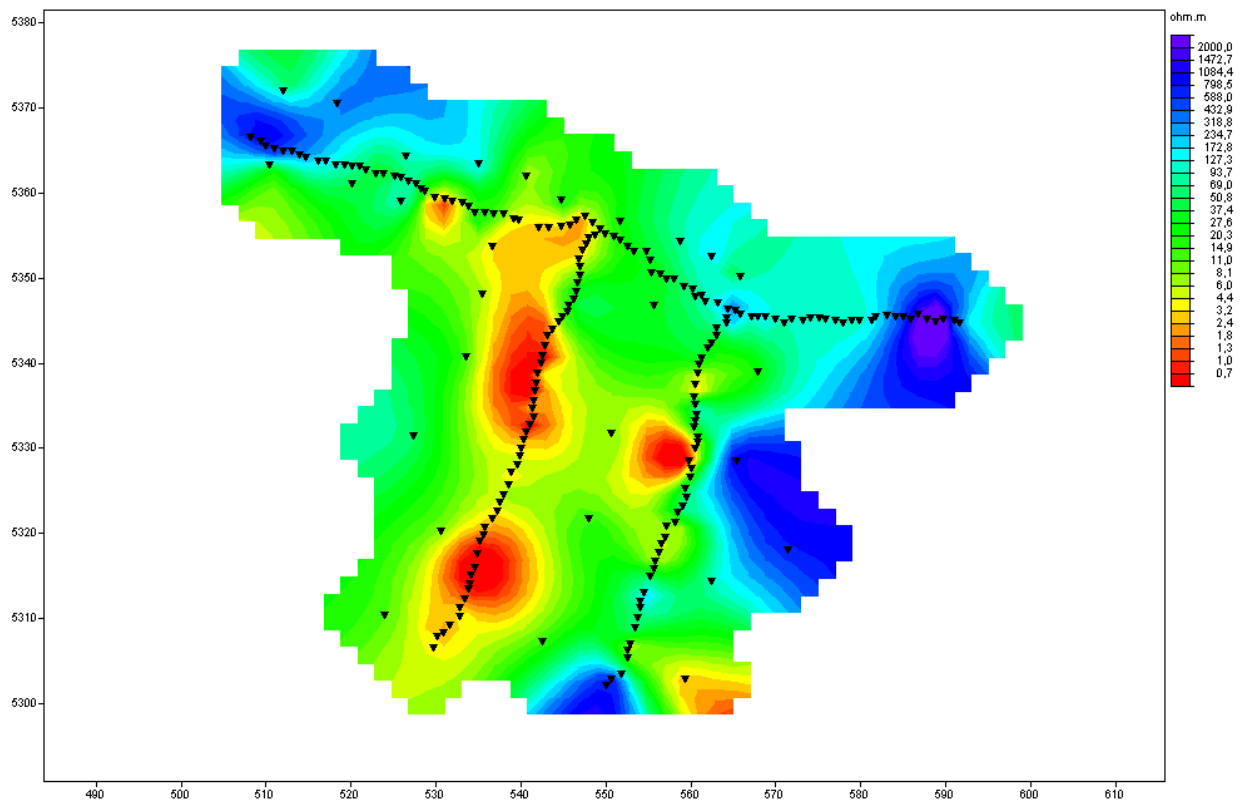


Figure 13. Plan slice of interpolated resistivity values from 2D models obtained by joint inversion of TE and TM data (-4 km a.s.l.).

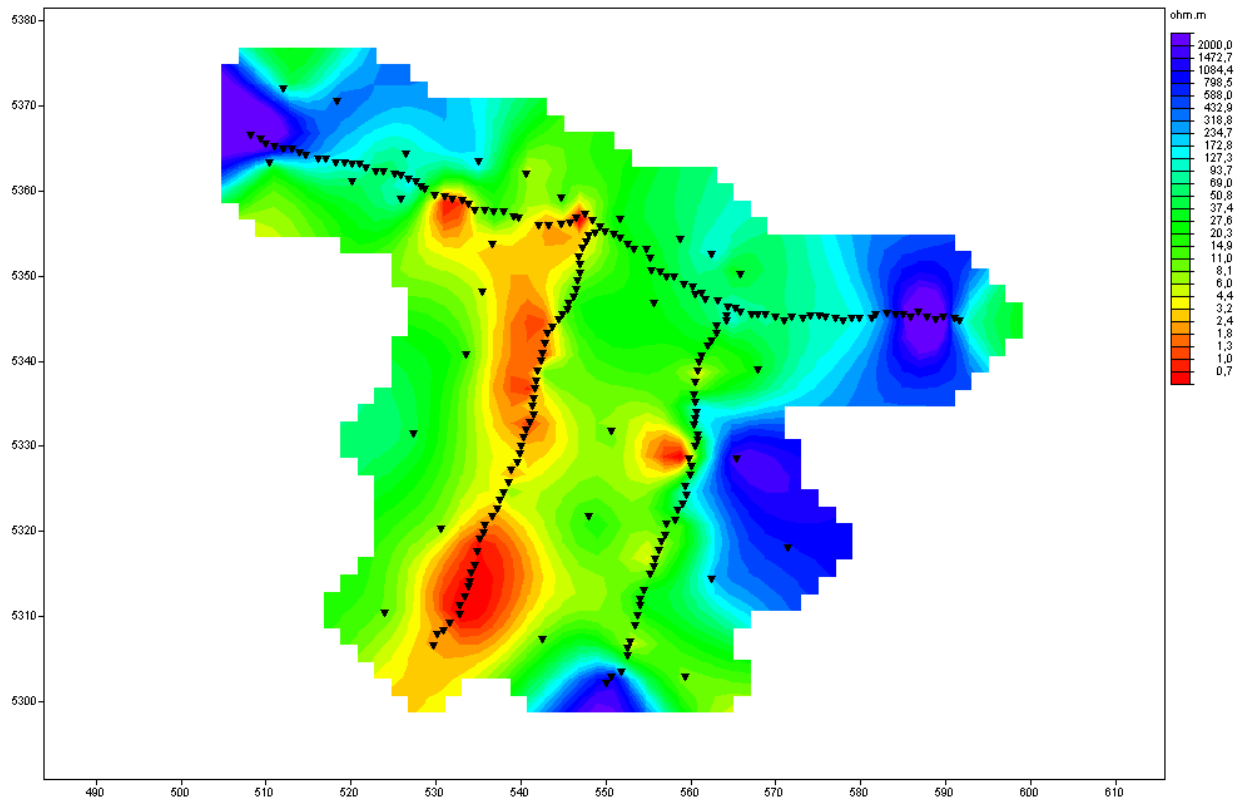


Figure 14. Plan slice of interpolated resistivity values from 2D models obtained by joint inversion of TE and TM data (-5 km a.s.l.).

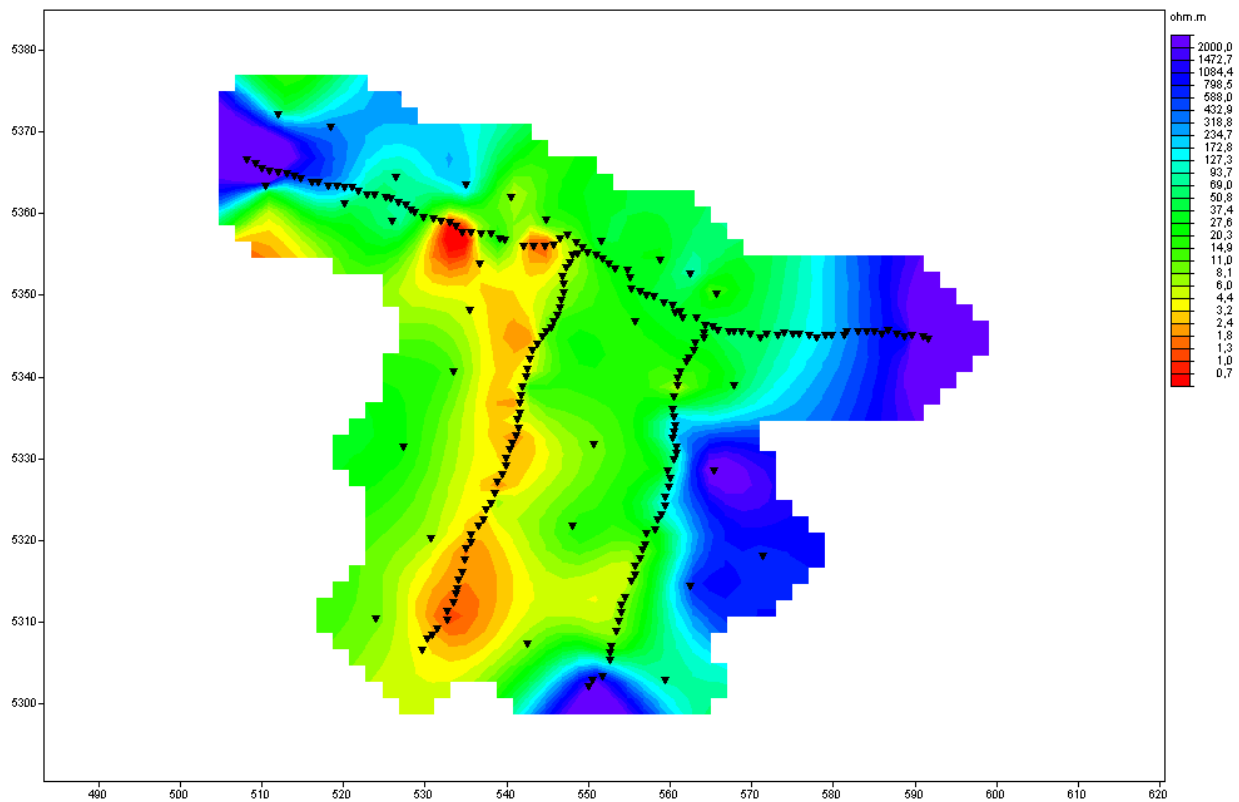


Figure 15. Plan slice of interpolated resistivity values from 2D models obtained by joint inversion of TE and TM data (-6 km a.s.l.).

Considerations

Results have proved what was already seen in the previous report, i.e., that the area shows a clear 3D structure and that a conductive anomaly is present on the western side of the original southern Profile (now part of A_2 Profile). Other conductive anomalies have been found in the area, by B_2 and B_4 profile data. The other profiles have too sparse sites to be able to define the details of these anomalies, but confirm the presence of a general resistivity reduction at depth.

The models I obtained are similar but not equal to those retrieved by 3D inversion modeling. This is mostly due to a better performance of 3D modeling in a 3D subsurface resistivity distribution, as attested also by the much lower RMS values of 3D with respect to 2D. However I wonder how the RMS values I read in the report for 3D can be so low with error floor of 3%. It would be interesting to compare the edited data we used for the inversion.

What surprised me, and took so much effort in modeling and trials, is the difference of results on what I named B_2 profile. With the data I am using I obtain a much broader conductive anomaly along this profile, which is very robust in my modeling tests. On the other side, along B_4 profile, the anomaly I define on the southern part is smaller than what defined in the 3D results.

What is evident by the inversion is that the resistive boundary of the area is much closer on the east (profile B_5, which looks more resistive in the TE-TM inversion) than it is on the west (profile B_1). Another consideration I want to highlight is that the higher resistivity of certain areas could be due not only to reduced permeability of rocks, but also to preferential paths of cold, meteoric fluid circulation. Some of the many fractures and faults defined by magnetic lineaments play an important role in the circulation of hot, but also cold water circulation at depth. It is very important to distinguish between the two, and to use resistivity information to derive a picture of the whole circulation pattern. This is possible by integration of MT with other data: for example gravity may distinguish between rocks of different permeability, but may not define if a fractured area is filled with hot or cold fluids; geology may provide the inclination of fracture and faults so that a projected faults/fracture distribution at depth may be compared with the resistivity distribution (a comparison of surface lineaments with resistivity anomaly at some km depth may result very biased if fractures and faults are not vertical). Data integration is the key for the complete analysis of MT, as well as all available, data.